

Conductance relaxation in GeBiTe - slow thermalization in an open quantum system.

Z. Ovadyahu

Racah Institute of Physics, The Hebrew University, Jerusalem 91904, Israel

Abstract

This work describes the microstructure and transport properties of GeBi_xTe_y films with emphasis on their out-of-equilibrium behavior. Persistent-photoconductivity (PPC), previously studied in the phase-change compound GeSb_xTe_y is also quite prominent in this system. Much weaker PPC response is observed in the pure GeTe compound and when alloying GeTe with either In or Mn. Films made from these compounds share the same crystallographic structure, the same p-type conductivity, a similar compositional disorder extending over mesoscopic scales, and similar mosaic morphology. The enhanced photoconductive response exhibited by the Sb and Bi alloys may therefore be related to their common chemistry. Persistent-photoconductivity is observable in GeBi_xTe_y films at the entire range of sheet resistances studied in this work ($\approx 10^3\Omega$ to $\approx 55\text{M}\Omega$). The excess conductance produced by a brief exposure to infrared illumination decays with time as a stretched-exponential (Kohlrausch law). Intrinsic electron-glass effects on the other hand, are observable in thin films of GeBi_xTe_y only for samples that are strongly-localized just like it was noted with the seven electron-glasses previously studied. These include a memory-dip which is the defining attribute of the phenomenon. The memory-dip in GeBi_xTe_y is the widest amongst the germanium-telluride alloys studied to date consistent with the high carrier-concentration $N \geq 10^{21}\text{cm}^{-3}$ of this compound. The thermalization process exhibited in either, the PPC-state or in the electron-glass regime is sluggish but the temporal law of the relaxation from the out-of-equilibrium state is distinctly different. Coexistence of the two phenomena give rise to some non-trivial effects, in particular, the visibility of the memory-dip is enhanced in the PPC-state. The relation between this effect and the dependence of the memory-effect magnitude on the ratio between the interparticle-interaction and quench-disorder is discussed.

PACS numbers: 72.20.-i 72.40.+w 78.47.da 72.80.Ng

INTRODUCTION

The approach to equilibrium of quantum systems is a fundamental problem that has received wide theoretical attention, mostly in close systems [1, 2]. Thermalization of open systems is a less researched subject although it is relevant for most naturally occurring processes. This is the case for out-of-equilibrium electronic transport in solids where coupling to a heat-bath via phonons usually plays a role at any finite temperature. In metals and semiconductors the rate of electron-phonon (e-ph) inelastic scattering γ_{in} may be appreciable; even at sub-Kelvin temperatures γ_{in} is typically $10^4\text{-}10^6\text{s}^{-1}$ at 1K [3]. An efficient e-ph coupling is the main reason for the fast relaxation of the electronic system after it has been taken out of equilibrium by a light-pulse or by Joule-heating it.

There are however situations where electronic relaxation is a sluggish process despite the presence of phonons; persistent photoconductivity (PPC), and the relaxation exhibited by electron-glasses are examples for such cases. In both phenomena the electronic conductance G is enhanced in their out of the equilibrium state, and in both the relaxation of G from the excited state may be a very slow process that may be monitored over time scales that are many orders of magnitude longer than phonon relaxation times. The slow relaxation associated with these phenomena make systems that exhibit them prime candidates for experimentally studying thermalization in open quantum systems.

PPC has been observed in lightly-doped semiconductors with carrier-concentration N typically smaller than

10^{18}cm^{-3} [4–8]. Recently this phenomenon was observed in GeSb_xTe_y alloys, p-type degenerate semiconductors with $N \approx 10^{20}\text{cm}^{-3}$ [9]. When Anderson localized, samples of GeSb_xTe_y exhibited both intrinsic [10] electron-glass effects and PPC. The interplay of the two coexisting phenomena showed non-trivial effects [10, 11].

In this work we discuss attempts to obtain similar results for other systems based on GeTe by incorporating either In, Mn, or Bi as the third element in the alloy. Despite the high concentration of these chemically different foreign elements, the resulting ternary compounds shared the same crystallographic structure and p-type conductivity of the GeTe parent compound. On the other hand, the transport properties differed markedly among the produced alloys, in particular in terms of their PPC performance. Incorporating In or Mn atoms in the GeTe matrix did not seem to affect the PPC of the pure compound. Bismuth however, proved to give enhanced PPC effects similar to the behavior of the phase-changed material GeSb_xTe_y [10]. In addition, GeBi_xTe_y samples appear to be an efficient system for studying transport effects associated with the interplay between disorder and interactions: The material is easy to fabricate, it is flexible in terms of being able to vary its disorder over a wide range including driving it insulating without making it granular. The bulk of the work described below is mostly devoted to the results obtained with this system.

The persistent photo-conductivity and electron-glass features may be separately observed in GeBi_xTe_y samples and exhibit their distinct relaxation laws. When these phenomena coexist, on the other hand, the electron-

glass features may be significantly modified, in particular, the memory-dip seems to have a larger magnitude in the PPC-state. It is argued that the ratio between the quench-disorder and inter-particle interaction plays a role in the visibility of the memory-dip. All other things being equal, this ratio is larger when the carrier-concentration N of the electron-glass is higher, which consistently results in a smaller magnitude of the memory-dip. However, in the PPC-state the interparticle-interaction to disorder ratio actually increases relative to the dark-state thus, in turn, enhancing the memory-dip magnitude.

Details of sample preparation, characterization, and their various measurements techniques are described in the next section. The results and their discussion are given in section III.

EXPERIMENTAL

Sample preparation and characterization

Samples used in this study were prepared by co-depositing GeTe and either Bi, In, or Mn on room temperature substrates in a high-vacuum system (base pressure $0.8\text{-}1\times 10^{-7}\text{mbar}$). The GeTe (Equipment Support Company, USA) was e-gun deposited with rates of $0.6\text{-}1\text{\AA}/\text{second}$ while Bi, In, or Mn were evaporated from a Knudsen source with a rate chosen such that the alloy composition should be close to 1:1:1. Film thickness varied in the range $40\text{-}60\text{\AA}$ for the films measured in this work. Lateral dimensions of the samples used for transport measurements were $0.3\text{-}0.5\text{mm}$ long and 0.5mm wide.

Two types of substrates were used; 1mm -thick microscope glass-slides, and $1\mu\text{m}$ SiO_2 layer thermally grown on $\langle 100 \rangle$ silicon wafers. The Si wafers (boron-doped with bulk resistivity $\rho \simeq 2\times 10^{-3}\Omega\text{cm}$) were employed as the gate electrode in the field-effect measurements. The microscope glass-slides were mostly used for Hall-Effect measurements performed at room-temperatures. These revealed p-type carrier-concentration N in all these alloys. For the GeBi_xTe_y films, that were the main system used in this work, N varied in the range of $(6\text{-}9)\times 10^{21}\text{cm}^{-3}$.

Each deposition batch included samples for transport measurements, samples for Hall-effect measurements, and samples for structural and chemical analysis. For the latter study, carbon-coated Cu grids were put close to the sample during its deposition. These grids received the same post-treatment as the samples used for transport measurements.

Transmission-electron-microscopy (TEM), using the Philips Tecnai G2) were employed to characterize the films composition and microstructure.

Polycrystalline samples of $\text{Ge}(\text{M})_x\text{Te}_y$ (where M stands for either Bi, In, or Mn) were obtained by mounting

the as-deposited (amorphous) films on a hot-plate set to a temperature $T_H=470\pm 5\text{K}$ for ≈ 2 minutes during which the sample was crystallized.

A TEM micrograph and associated diffraction pattern of typical GeBi_xTe_y and GeMn_xTe_y films produced in the above manner are shown in Fig.1 and Fig.2 respectively. These TEM micrographs and diffraction patterns illustrate the polycrystalline nature of the films and a tight, space-filling packing of the crystallites. The main difference between the Bi and the Mn alloys is obviously their different grain-sizes. These are just few nanometers for the GeBi_xTe_y film as compared with $\approx 100\text{nm}$ for GeMn_xTe_y . Similar grain-sizes were observed in our GeIn_xTe_y films. The large disparity in grain-size is also reflected in the diffraction patterns (Fig.1 and Fig.2). Diffraction patterns taken from these films were consistent with the rhombohedral (R-3m) phase of GeTe in all samples made of the three ternary compounds.

Several types of structural defects may be observed in these micrograph; grain boundaries and twinning being the most prevalent. These defects, as well as the compositional-disorder (discussed next), and surface scattering are presumably responsible for restricting the mobility of the films.

The main difference between the GeBi_xTe_y and the GeMn_xTe_y and GeIn_xTe_y films is their mobility. For the thickness range of $40\text{-}60\text{\AA}$, the GeBi_xTe_y samples had sheet resistance R_{\square} in the range $2\text{k}\Omega\text{-}55\text{M}\Omega$ at 4K . With this range it was possible to cover a large part of the strongly-localized regime ($R_{\square} > h/e^2$) which is a pre-requirement for observing inherent electron-glass effects [12]. In contrast, we were not yet able to push R_{\square} much above $\approx 10^2\text{k}\Omega$ in samples made from either of the two other alloys even by deliberate surface-oxidation. This is presumably the reason for our failure to detect electron-glass effects in GeMn_xTe_y and GeIn_xTe_y films. The higher resistance obtainable in the GeBi_xTe_y alloy may be in part due to their much smaller grain-size as noted above. However, the grain-size in the previously studied GeSb_xTe_y [10] was even larger than in GeMn_xTe_y and GeIn_xTe_y and had more pronounced texture (which means less boundary scattering) than that observed in GeMn_xTe_y while films with $R_{\square} \geq 50\text{M}\Omega$ were easily produced even in thicker films [10]. Inter-grain scattering is therefore not likely to be the main source of disorder in these alloys.

The focus of this work is the difference between the two mechanisms for slow relaxation and therefore, in the following, data are shown mainly for the GeBi_xTe_y samples where both PPC and electron-glass effects are observable.

The stoichiometry of the GeBi_xTe_y films was measured by EDS (Energy Dispersive Spectroscopy) attachment of the TEM. Different preparation runs produced films that usually had the average stoichiometry close to the desired goal mentioned above. However, there was no-

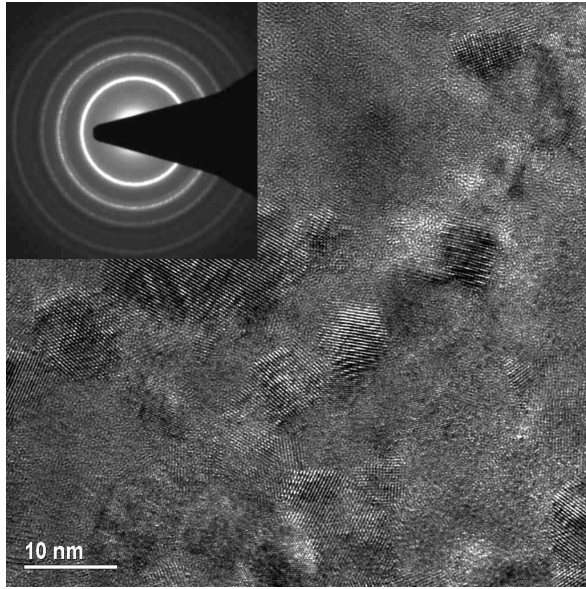


FIG. 1: Bright-field of a 5nm film of GeBi_xTe_y and an associated diffraction-pattern. The micrograph shows polycrystalline structure with grain-size of the order of 1-2nm which accounts for the rather uniform rings in the diffraction-pattern.

ticeable composition heterogeneity on a mesoscopic spatial scale. This kind of disorder is quite common in alloys and may be accompanied by spatial fluctuations in carrier-concentration [13]. A similar composition heterogeneity has been seen also in GeTe [14]. Figure 3 shows the distribution of local stoichiometry (on a mesoscopic 40nm scale) across a typical GeBi_xTe_y film. Composition variations may be accompanied by local variations of the carrier-concentration, and these are of particular importance in superconducting materials which are notoriously sensitive to the value of N . In the presence of disorder such inhomogeneities may lead to the appearance of superconducting islands embedded in an insulating matrix making it effectively a granular system [13]. One should be aware of these non-uniform structural aspects whenever the transport property one measures has a spatial scale that is smaller or comparable with the scale of the inhomogeneities.

Measurement techniques

Conductivity of the samples was measured using a two-terminal ac technique employing a 1211-ITHACO current preamplifier and a PAR-124A lock-in amplifier. Most measurements were performed with the samples immersed in liquid helium at $T \approx 4.1\text{K}$ held by a 100 liters storage-dewar. This allowed up to two months measurements on a given sample while keeping it cold (and in the dark). These conditions are essential for measurements where extended times of relaxation processes are required

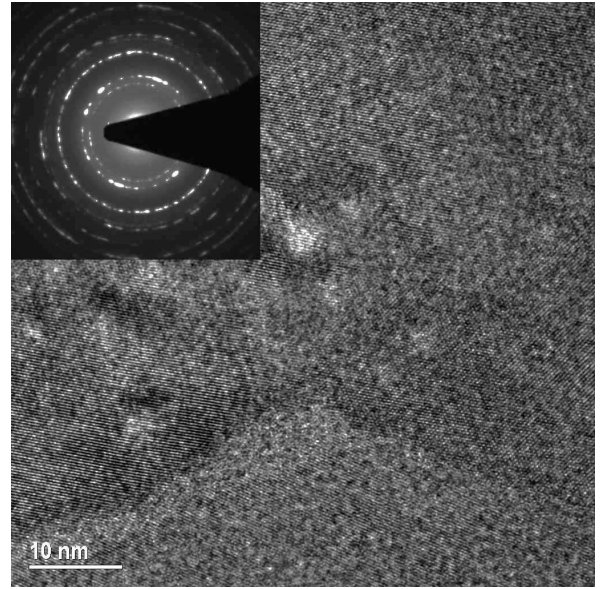


FIG. 2: Bright-field of a 5nm film of GeMn_xTe_y and an associated diffraction-pattern taken under similar conditions as the sample in Fig.1 (same selected-area for the diffraction pattern). The typical grain-size in this case is clearly much larger than in the GeBi_xTe_y sample. The relatively large grain-size in this case is also reflected in the "spotty" rings of the diffraction-pattern.

at a constant temperature.

The gate-sample voltage (to be referred to as V_g in this work) in the field-effect measurements was controlled by the potential difference across a $10\mu\text{F}$ capacitor charged with a constant current. The range of V_g used in this study reached in some cases $\pm 40\text{V}$ which is equivalent to the $\pm 20\text{V}$ used in previous work [15] where the gate-sample separation was $0.5\mu\text{m}$ of as compared with the $1\mu\text{m}$ SiO_2 spacer used here.

The ac voltage bias in conductivity measurements was small enough to ensure near-ohmic conditions (except for the current-voltage plots). Optical excitations in this work were accomplished by exposing the sample to an Al-GaAs diode operating at $\approx 0.88 \pm 0.05\mu\text{m}$ mounted on the sample-stage $\approx 10\text{-}15\text{mm}$ from the sample. The diode was energized by a computer-controlled Keithley 220 current-source.

RESULTS AND DISCUSSION

Field-effect measurements

Conductance versus gate-voltage $G(V_g)$ traces typical for diffusive GeBi_xTe_y samples are shown in Fig.4. The sign of $\partial G(V_g)/\partial V_g$ that characterize the field-effect of these weakly-disordered samples is consistent with band-structure calculations for GeTe and similar compounds

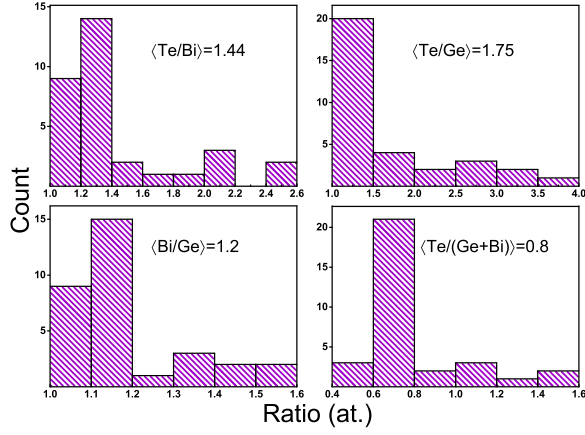


FIG. 3: Histograms of the atomic ratios for the three components of the GeBi_xTe_y sample shown in Fig.1 above. The histograms are based on 35 local EDS measurements across the film, each sampling the contribution from a $40 \times 40 \text{nm}^2$ area. Note that the most likely ratio is close to a composition of 1:1:1 but there is a significant scatter around this value. Note that the average ratio for Te/Ge deviates from unity while $\text{Te}/(\text{Ge}+\text{Bi}) \approx 1$ which may hint that the Bi atoms reside on Ge-sites in the crystal.

[16]. These theoretical models account for the p-type conduction in the material, in agreement with the sign of the Hall-Effect mentioned above. The Fermi-energy in this scenario appears at the top of the valence-band (see inset to Fig.4). Sweeping V_g changes the position of the Fermi-energy and the associated change in the conductance reflects the energy dependence of $\partial n/\partial \mu$, the thermodynamic density-of-states (DOS). The measured $G(V_g)$ is a convoluted outcome of $\partial n/\partial \mu(\varepsilon)$ and $D(\varepsilon)$ - the energy-dependent diffusion-constant. For all GeBi_xTe_y samples reported here, $\partial D/\partial \varepsilon > 0$ and is larger with larger R_{\square} as evidenced by the temperature dependence of their resistance; the resistance ratio $R(4\text{K})/R(300\text{K})$ is: 1.23, 2.37, and 3.43 for the films with $R_{\square} = 6.5\text{k}\Omega$, $32\text{k}\Omega$, and $110\text{k}\Omega$ in Fig.4 respectively. This explains the reason for the a general trend in the field-effect data of disordered conductors; $\partial G(V_g)/\partial V_g$ is a *monotonously increasing function* of R_{\square} .

Another feature appears in the $G(V_g)$ traces of GeBi_xTe_y samples that have large enough disorder. This usually requires that the sheet-resistance of the films R_{\square} be considerably larger than $h/e^2 \approx 25\text{k}\Omega$. Figure 5 shows $G(V_g)$ for a $\approx 50\text{M}\Omega$ film that was taken under the same conditions (temperature, sweep-rate) as the samples in Fig.4. The new feature is a local depression of $G(V_g)$ centered, in this case, at $V_g = 0\text{V}$. This feature is the memory-dip, a characteristic signature of the electron-glass [17–21]. It is believed to be a modulation of $g(\varepsilon)$, the *single-particle* DOS resulting from inter-particle correlations [22–25].

A modulation of $g(\varepsilon)$ due to correlation effects oc-

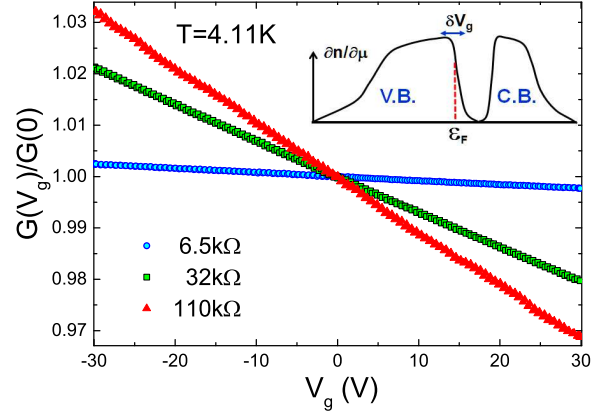


FIG. 4: $G(V_g)$ traces for three GeBi_xTe_y films showing nearly perfect linear dependence on the gate-voltage V_g with a slope that increases with R_{\square} . The inset is a schematic depiction of the band structure of the material and the position of the Fermi-energy.

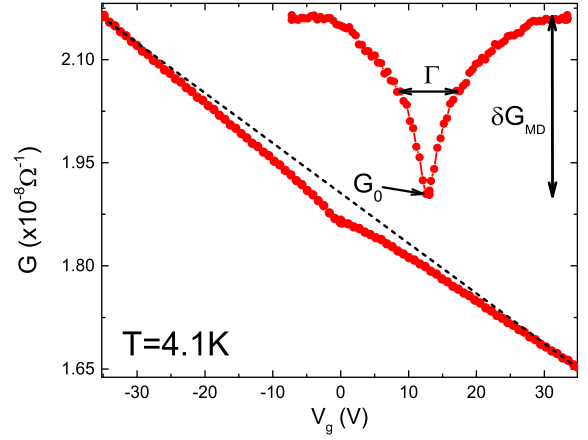


FIG. 5: Conductance versus gate-voltage for a GeBi_xTe_y film with $R_{\square} = 53\text{M}\Omega$. This $G(V_g)$ trace was taken 24 hours after the sample was allowed to equilibrate under $V_g = 0\text{V}$. The dashed line stands for the thermodynamic density-of-states which, consistent with the data in Fig.4 is assumed to be linear. The inset to the figure shows the memory-dip of this sample obtained by subtracting the thermodynamic DOS (the linear part of $G(V_g)$ taken for this sample). The memory-dip plot is marked with arrows to define its typical width Γ , its magnitude δG_{MD} and the "equilibrium" value of the conductance, G_0 .

curr in disordered conductors even in the diffusive regime where field-effect measurements would reveal just the thermodynamic component $\partial n/\partial \mu$. The contribution of a single-particle DOS may be reflected in tunneling or photo-emission processes but it is not expected to show up in a thermodynamic measurement such as field-effect [26]. This however is because V_g is usually swept sufficiently slow to allow the electronic system to be in equilibrium. When the equilibration time of the system becomes longer than the inverse sweep-rate (a condition

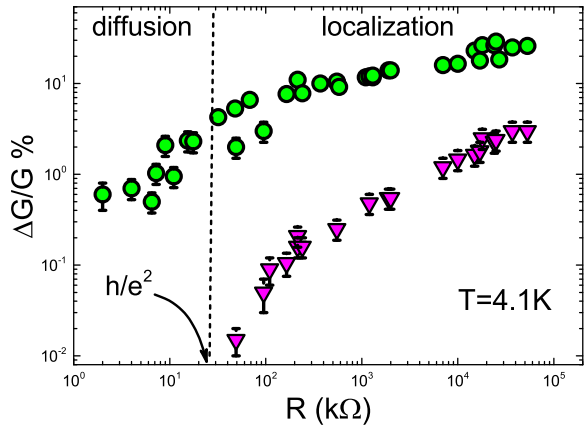


FIG. 6: Comparing the magnitude of the memory-dip (triangles) and slope of the thermodynamic density-of-states (circles) for several GeBi_xTe_y films. For the latter the value for $\Delta G/G$ is based on: $G(-30\text{V})/G(+30\text{V})$.

that is met in the electron-glass regime of highly disordered Anderson insulators [27]), the underlying $g(\varepsilon)$ would manifest itself in the $G(V_g)$ plot. The shape of this modulation, and its dependence on temperature, have been discussed by Lebanon, and Müller [23]. The magnitude of the memory-dip (defined in Fig.5), that will be referred to in this paper as ‘visibility’, depends therefore on how fast the gate-voltage is swept. This was demonstrated in field-effect experiments on crystalline indium-oxide [12]. The slope of the thermodynamic component of $G(V_g)$, on the other hand, is independent of $\partial V_g/\partial t$ [12].

The relative magnitude of the memory-dip $\delta G_{\text{MD}}/G_0$, increases with R_{\square} as illustrated in Fig.6 for the GeBi_xTe_y films studied in this work. The average slope of $G(V_g)$ for this samples is plotted on the same graph for comparison.

The qualitative features of these data are remarkably similar to those obtained on the half-a-dozen previously studied electron glasses [27]. In particular, they all show fast decline of the memory-dip magnitude as the diffusive regime is approached from the strongly-localized side, and a similar functional dependence of $\delta G_{\text{MD}}/G_0$ on R_{\square} . This re-enforces the conclusion that strong-localization is a pre-requisite for observing electron-glass effects.

Another feature that appears to be common to electron-glasses is the dependence of their memory-dip width Γ on the carrier-concentration N . A comparison of the memory-dip width and the carrier-concentration for the three germanium-telluride compounds studied to date is given in Fig.7. This shows a monotonous increase of Γ with the inter-particle separation $N^{-1/3}$. A similar dependence was found in the early work on amorphous indium-oxide [28] which hitherto was the only system where $\Gamma(N)$ was studied over a meaningful range of N . It would be interesting to be able to extend the range of the

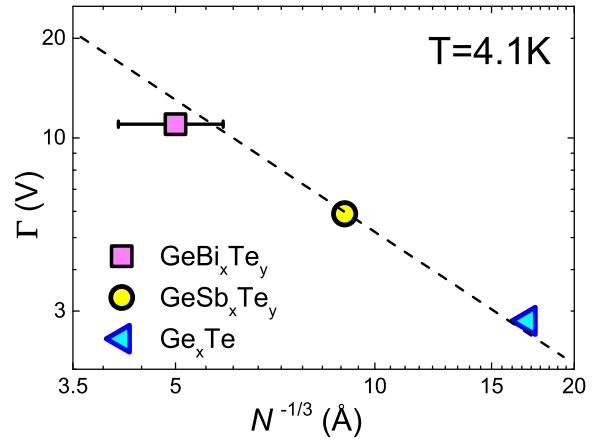


FIG. 7: The width of the memory-dip Γ (defined in Fig.5) for three germanium-telluride alloys as function of their carrier-concentration N . The value for Γ (defined in the inset to Fig.5) is based on $G(V_g)$ measurements at $T=4.1\text{K}$ and a SiO_2 layer of $0.5\mu\text{m}$ separating the sample for the gate.

carrier-concentration in the GeTe system towards lower N values to see whether the relaxation time becomes very short below a certain concentration as it does in In_xO [28].

Quantitatively however there are some features that distinguish the GeBi_xTe_y samples from previously studied electron-glasses. In particular, the magnitude of the memory-dip $\delta G_{\text{MD}}/G_0$ is relatively small when compared with the magnitude of the slope of the thermodynamic density-of-states $\partial n/\partial \mu$ for a given R_{\square} (Fig.6). This is mainly due to the steep dependence of $\partial n/\partial \mu$ on energy of this material. This makes it harder to observe the memory-dip in the $G(V_g)$ traces than in e.g., beryllium [29] that has a similar magnitude of $\delta G_{\text{MD}}/G_0$ for the same R_{\square} . The latter is still considerably smaller than exhibited by electron-glasses with lower carrier-concentrations N , $\text{In}_2\text{O}_{3-x}$ and In_xO (with $N < 10^{20}\text{cm}^{-3}$), a point that will be addressed later in this paper.

As is clear from Fig.6, a memory-dip could be observed only in strongly insulating samples. The conductance G of these samples, like all other electron-glasses, exhibit exponential temperature dependence of conductivity. Temperature dependence of G is shown in Fig.8 for two of the studied GeBi_xTe_y samples.

It is interesting to compare these $G(T)$ with the respective data of another electron-glass, $\text{In}_2\text{O}_{3-x}$ which has structural features that are similar to GeBi_xTe_y . Both show a mosaic, polycrystalline structure. Insulating $\text{In}_2\text{O}_{3-x}$ films with comparable value of R_{\square} exhibit a behavior consistent with Mott-type hopping in two-dimensions; $G(T) \propto \exp[-(T_0/T)^{1/3}]$ [30] rather than the simple activation $G(T) \propto \exp[-T_0/T]$ shown by GeBi_xTe_y over the same temperature range (Fig.8). As noted above, a pre-condition for showing electron-glass properties is strong-localization, and one of the characteristic

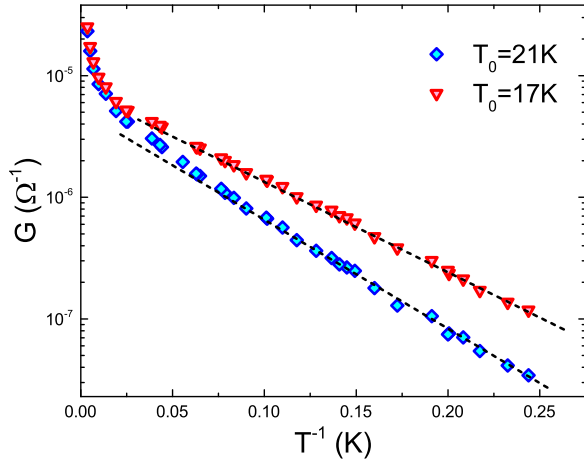


FIG. 8: Conductance versus temperature for two GeBi_xTe_y samples used in the study with thickness of 45\AA and $R_{\square}=8.5\text{M}\Omega$ and $R_{\square}=30\text{M}\Omega$ at $T=4.1\text{K}$. Samples are labeled by their activation-energies taken from the respective $R(T) \propto \exp[T_0/T]$ data.

features of this state is an exponential $G(T)$. However, the specific form of this function, and the structural details of the system appear to be unimportant. In other words, the features of electron-glasses may not be identified by the specific form their $G(T)$ takes. An exponential $G(T)$ whether simple activation or of the stretched-exponential kind is a necessary condition but, for observing the memory-dip in field-effect measurement other requirements have to be met, in particular strong disorder [27].

GeBi_xTe_y and $\text{In}_2\text{O}_{3-x}$ differ also in their sensitivity to applied electric fields; non-ohmicity in hopping systems often sets in at rather small fields at liquid helium temperatures [31–34] and the present system is no exception; R_{\square} as function of the applied voltage V are plotted in Fig.9 for four GeBi_xTe_y samples with different degrees of disorder clearly show the common trend.

Susceptibility to non-ohmic behavior is more conspicuous in $\text{In}_2\text{O}_{3-x}$ than in the GeBi_xTe_y films: To illustrate, $\text{In}_2\text{O}_{3-x}$ sample with $R_{\square}=12.5\text{M}\Omega$ decreased by $\approx 90\%$ upon applying a field of 10V/cm at $T=4.1\text{K}$ [37] while under the same conditions the drop of R_{\square} is a mere 2.4% for the GeBi_xTe_y film with $R_{\square}=15\text{M}\Omega$ (Fig.9).

Non-ohmicity deep in the hopping regime is mainly caused by a field-assisted mechanism [31–34] but Joule-heating is an accompanying factor; for a given applied field the relative importance of heating would become larger when the resistance is smaller. The higher sensitivity of $\text{In}_2\text{O}_{3-x}$ to the applied field is related to the compounded effect of both mechanisms. As a low N system the hopping-length for a given temperature and resistance is likely longer than in the GeBi_xTe_y system which makes the field-assisted mechanism stronger for a comparable field strength. The heating sensitivity of the

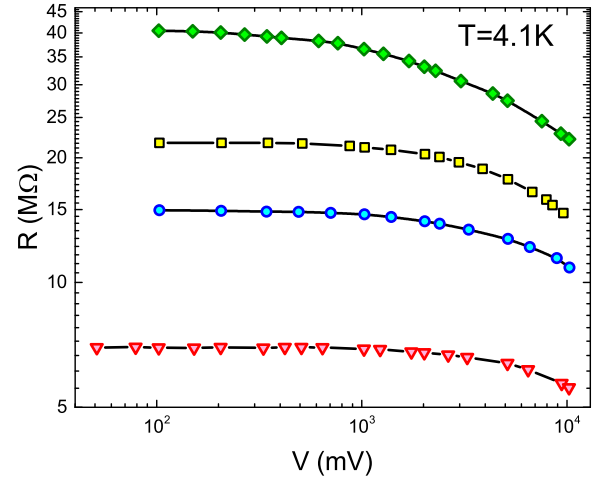


FIG. 9: The dependence of sample resistance on the longitudinal voltage for GeBi_xTe_y films with different disorder. Samples shown had a common geometry of 0.5mm length and 0.5mm width.

conductance involves (among other things) the electron-phonon inelastic-scattering rate. This is likely to be more important in $\text{In}_2\text{O}_{3-x}$ due to its unusually large Debye temperature [36]. In any case, the larger range of applied voltages over which linear-response condition may be maintained using GeBi_xTe_y samples should be a convenient feature for experimental study of hopping conductivity.

There is another feature of GeBi_xTe_y that may make it a versatile test-bed for a variety of non-equilibrium phenomena; GeBi_xTe_y films exhibit pronounced response to photo-excitation. Just like it was observed in GeSb_xTe_y films [9, 11], exposure to infrared illumination increased the samples conductance by a certain ΔG which persisted long after the light source was turned off. The experimental protocol used for optical excitation is illustrated in Fig.10. The experiment typically begins ≈ 24 hours after the sample is cooled-down to 4.1K by recording $G(t)$ for 1-2 minutes to establish a baseline, near-equilibrium conductance G_0 . The IR source was then turned on for 3 seconds and then turned off while $G(t)$ continues to be measured.

The figure depicts the conductance dependence during excitation and the ensuing relaxation following its termination. The latter has a characteristic time dependence that fits a stretched-exponent law:

$$G(t) \propto \exp[-(t/\tau)^\beta] \quad (1)$$

(see inset to Fig.10). This is a manifestation of persistent photoconductivity (PPC), a phenomenon that has been frequently observed in many semiconductors [3–8] and recently found in the compound GeSb_xTe_y [9, 11].

In general, the relative change of the conductance due

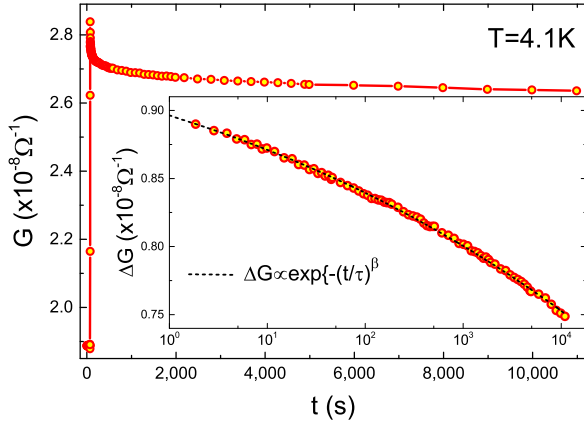


FIG. 10: Conductance evolution during a typical optical excitation protocol. The sample is a 43\AA thick GeBi_xTe_y with equilibrium $R_{\square}=53\text{M}\Omega$ at 4.1K . It is exposed to the infrared LED operated with 1mA for 3s at a distance of $\approx 9\text{mm}$ from the sample. The conductance is monitored for $11,000\text{s}$ after the LED is turned off during which time it decays slowly with a stretched-exponential law as depicted in the inset. A fit to $\Delta G(t) \propto \exp[-(t/\tau)^\beta]$ with $\tau=1.3 \times 10^9\text{s}$ and $\beta=0.11$ is shown in the inset as a dashed line.

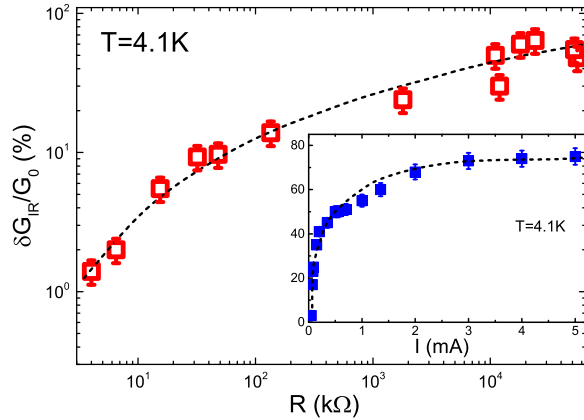


FIG. 11: The relative increase of conductance due to a brief infrared exposure $\delta G_{\text{IR}}/G_0$ plotted as function of the sheet resistance of the sample. G_0 is the equilibrium value of the conductance and δG_{IR} is arbitrarily chosen as $\delta G_{\text{IR}}=G(t=3 \times 10^3)-G_0$. The inset shows the dependence of $\delta G_{\text{IR}}/G_0$ on the infrared intensity for a typical sample. Dashed lines are guides for the eye.

to the brief infrared exposure $\delta G_{\text{IR}}/G_0$ increases with R_{\square} as shown in Fig.11.

The same energy-flux (1mA current through the infrared diode for 3s) was delivered to all samples in the series with sheet-resistances of $4\text{k}\Omega$ to $55\text{M}\Omega$. This value was chosen after studying the dependence of the effect on the excitation current shown in the inset to Fig.11. The excitation by 1mA was chosen as a compromise between achieving an appreciable δG_{IR} while minimizing heating and associated detrimental effects to the electron-glass state which may coexist with the PPC when the system

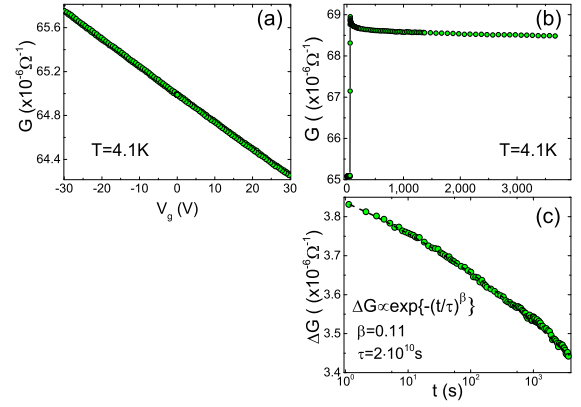


FIG. 12: Data for a field-effect measurement (a) and infrared excitation protocol (b and c) for a diffusive GeBi_xTe_y sample with thickness 50\AA and $R_{\square}=15.4\text{k}\Omega$ at $T=4.1\text{K}$. Note the linear $G(V_g)$ trace in (a) consistent with diffusive behavior. Plate (c) illustrates the fit to the relaxation law where the time origin is taken to coincide with the turning off of the infrared LED.

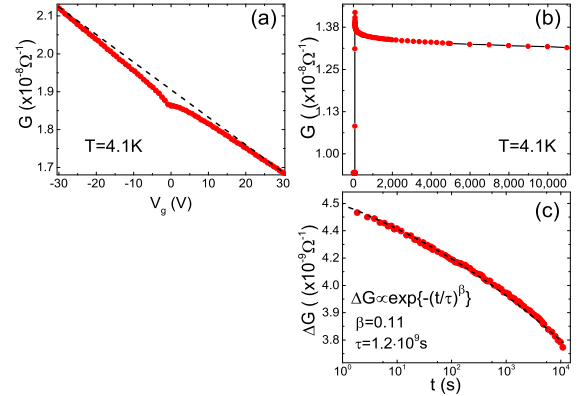


FIG. 13: Data for a field-effect measurement (a) and infrared excitation protocol (b and c) for a strongly-localized GeBi_xTe_y sample with thickness 48\AA and $R_{\square}=57\text{M}\Omega$ at $T=4.1\text{K}$. Note the appearance of a memory dip in the $G(V_g)$ trace (a) consistent with insulating behavior. Plate (c) illustrates the fit to the relaxation law where the time origin is taken to coincide with the turning off of the infrared LED.

is in the strongly-localized regime.

The detailed behavior of the PPC in the GeBi_xTe_y films turns out to be similar to that of GeSb_xTe_y [9, 11]; in both systems PPC is observable in samples that are in the diffusive regime as well as in strongly-localized samples. The relaxation law associated with PPC is essentially the same for a diffusive sample (Fig.12) and for a strongly-localized sample (Fig.13). The latter is in the electron-glass phase and exhibits a well-developed memory-dip whereas the $G(V_g)$ the diffusive sample reveal only the thermodynamic DOS in the field-effect scan.

These two alloys are also similar in terms of magnitude and fit parameters to the stretched exponential relax-

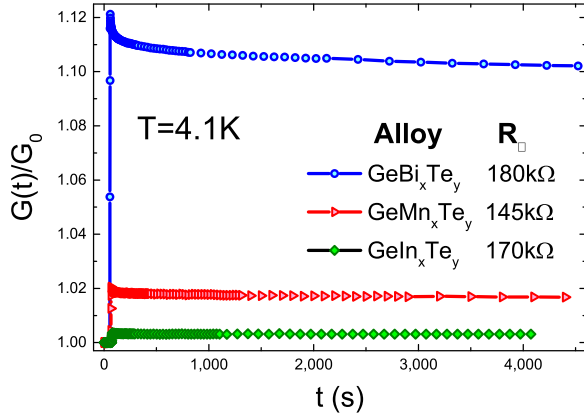


FIG. 14: Comparing the result of the infrared excitation protocol for three germanium-telluride alloys. The same protocol conditions were used in each case as specified in Fig.10.

ation law. The $G(t)$ measured following the infrared excitation of the samples shown in Fig.11 could be fitted to Eq.1 with the same $\beta = 0.11 \pm 0.005$ as a best-fit parameter. The other fit parameter in the stretched-exponential law is τ that is found to be of order 10^9 sec to 10^{10} sec in all our samples. There was no systematic dependence of τ on the sample sheet resistance R_{\square} . Similar values for β and the relaxation-time τ were found at these temperatures in the relaxation law of PPC in $\text{AlGa}_x\text{As}_{1-x}$ compounds [5] and in the GeSb_xTe_y films studied previously [9, 11].

Applying the infrared protocol to GeMn_xTe_y and GeIn_xTe_y samples resulted in a considerably lower $\delta G_{\text{IR}}/G_0$ values as compared with GeSb_xTe_y and the GeMn_xTe_y samples with similar resistances. A comparison between the response of GeMn_xTe_y and GeIn_xTe_y samples with GeBi_xTe_y films is shown in Fig.14.

The $G(t)$ plots of the infrared protocol for these samples plotted in Fig.14 are the highest in terms of the magnitude of δG_{IR} obtained so far. The overall appearance of these relaxation curves appear to be similar to those of the GeBi_xTe_y and GeSb_xTe_y alloys but the signal-to-noise of the $G(t)$ data are not yet good enough to allow for a reliable determination of β and τ for either GeMn_xTe_y or GeIn_xTe_y . In addition, there were appreciable fluctuations in the magnitude of $\delta G_{\text{IR}}/G_0$ taken from different preparation batches of these alloys. This may indicate that the PPC in GeMn_xTe_y and GeIn_xTe_y (as well as in the parent compound GeTe) results from the spurious occurrence of a defect and that the enhanced PPC response in the GeBi_xTe_y and GeSb_xTe_y is due to a catalytic effect of incorporating Bi or Sb in the ternary alloy.

Our persistent-photoconductivity results in these GeTe alloys resembles in many aspects the behavior reported in compounds based on PbTe, a system that has been extensively studied [4]. In particular, the sensitivity of

the PPC magnitude to the specific chemistry of the element added to the alloy seems to be a common feature (the dopants that yield higher PPC efficiency are however different).

The similar dynamics of the GeBi_xTe_y and the GeSb_xTe_y alloys in their PPC-state may be an important clue for unraveling the nature of the defect responsible for the long-lived PPC state. While the involvement of a massive defect is believed to be a key element in most models for the PPC phenomenon [4], the basic question is whether the relevant defect is the added element itself (Sb or Bi in our case) or it is an indirect result of its presence in the alloy [4]. Given the substantial difference in the masses of Sb and Bi, one would argue that the similar parameters of the relaxation dynamics in the PPC-state of GeBi_xTe_y and GeSb_xTe_y as well as the similar behavior of the undoped GeTe, favor the indirect scenario.

Modification of the electron-glass behavior in the PPC state

Strongly-localized samples of GeBi_xTe_y exhibit all the qualitative nonequilibrium features found in previously studied electron-glasses. These are distinguishable from the PPC observed in this system in a number of aspects. First and foremost, as mentioned above, unlike persistent photoconductivity, the electron-glass features are not observed in the diffusive regime of the system. Secondly, there are more ways to take the electron-glass far from the equilibrium than just by exposure to electromagnetic radiation; stressing the sample with longitudinal field [38], and changing the density of carriers in the system (via a change of the gate-voltage), are two examples for unique ways to take the system away from equilibrium. Finally, the relaxation-law towards equilibrium of the conductance is logarithmic with time for the electron-glass as compared with the stretched-exponential law for PPC. Figure 15 illustrates two of the above distinguishing features of the electron-glass.

Some electron-glass features are significantly modified when coexisting with persistent photoconductivity. This is not surprising; the "persistent" mode is not a stationary-state, the concentration of charge-carriers continuously diminishes with time, and this has consequences. It is easy to understand that in the PPC-state the relaxation law of the electron-glass would appear different because the background conductivity is decaying with a stretched-exponential law. Figure 16 demonstrates such a case using the gate-protocol to drive the electron-glass away from "equilibrium" while the system is still relaxing from the infrared exposure applied several hours before.

The main effect of the combined relaxation in this case is a modified relaxation-law that deviates from the $\log(t)$ dependence that characterizes the electron-glass.

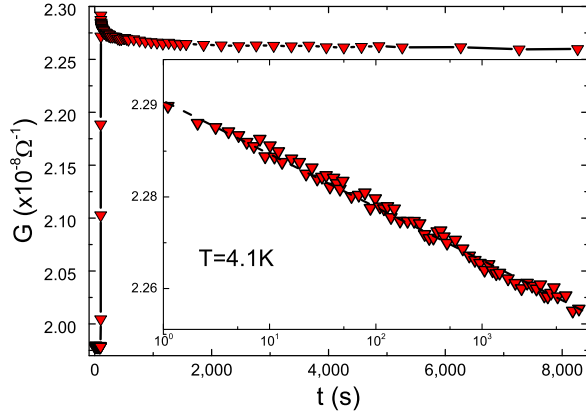


FIG. 15: Conductance evolution during excitation protocol using a sudden change of gate-voltage. The sample is a 43Å thick GeBi_xTe_y with "dark" $R_{\square}=53\text{M}\Omega$ at 4.1K. It was allowed to relax under $V_g=0\text{V}$ for 40 hours and after recording its "equilibrium" G_0 for $\approx 10^2\text{s}$, V_g was swept to -35V within 3.5s producing the $G(t)$ data shown in the figure. The inset illustrates that, after the new $V_g=-35\text{V}$ is established, the sample conductance decays with a logarithmic time dependence. Dashed line is best fit for a $G(t)=G(1)-a\cdot\log(t)$ law.

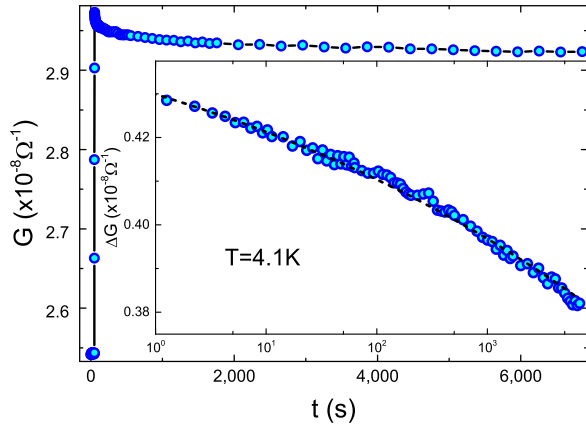


FIG. 16: Conductance evolution during excitation by a gate protocol using the same parameters as in Fig.15 except that the sample was first put in its PPC-state as per the infrared protocol (Fig.10). The system was then allowed to relax for three hours before changing the gate voltage. The inset illustrates that, after the new $V_g=-35\text{V}$ is established, the sample conductance decays with a stretched-exponential time dependence. Dashed line is best fit for a $G(t)\propto\exp[-(t/\tau)^\beta]$ with $\beta=0.11$ and $\tau=3\cdot 10^{10}\text{s}$.

The total change of ΔG observed during the $\approx 7,000$ seconds, over which data are plotted in Fig.16, is comparable in magnitude to the sum of the respective ΔG 's estimated from the relaxations due to the PPC and the electron-glass (assuming that each is present without the other). This assumption however cannot be accurate; coexistence of the two nonequilibrium phenomena manifestly produces effects that are not consistent with simple superposition. This is demonstrated in the experiment

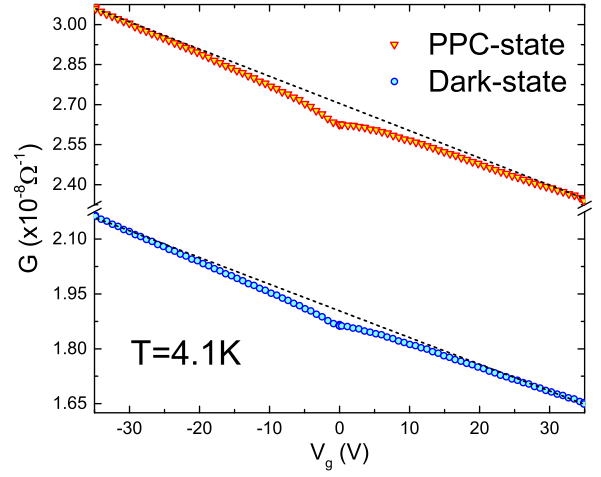


FIG. 17: Field-effect $G(V_g)$ traces for a GeBi_xTe_y sample with "dark" $R_{\square}=54\text{M}\Omega$ taken 24 hours after cooldown to $T=4.1\text{K}$ (circles) and 3 hours after exposing the film to infrared radiation at 1mA for 3s (squares). Both traces were taken with the same sweep rates of 0.023V/s. The relative slopes $\Delta G/G$ of the thermodynamic component of $G(V_g)$ (see Fig.6 for definition) were $\approx 30\%\pm 0.1\%$ for both curves while the magnitude of the memory-dip $\delta G_{\text{MD}}/G_0$ is $2\%\pm 0.1\%$ in the dark-state and $2.9\%\pm 0.1\%$ in the PPC-state.

described in Fig.17. The figure compares $G(V_g)$ for a GeBi_xTe_y film before and after being exposed to the infrared source yielding a counter-intuitive result: The sample under the PPC-state exhibits a *larger* amplitude of the memory-dip than the same film in its "dark" state.

This is not a trivial result; it is natural to expect that exposing the electron-glass to infrared radiation would result in a *diminishment* of the memory-dip magnitude. In fact, it has been shown that above a certain threshold of energy-flux, infrared illumination may completely erase the memory-dip [39]. The energy flux associated with initiating the PPC-state is much smaller than used in [39] but the enhancement of the memory-dip is still an unexpected result.

A similar effect in GeSb_xTe_y was ascribed to the presence of a series-resistor that is reduced in the PPC-state [9, 11]. This was motivated by the observation of the concomitant increase of the slope of $\partial n/\partial \mu(\epsilon)$. However, this approach was not able to account for the magnitude of the enhancement. Besides, the lack of change in the slope of the thermodynamic DOS in the present case [see Fig.17], makes this line of explanation questionable anyhow (although, given the inhomogeneous structure, part of the effect might be related to reduction of a series resistor).

An alternative scenario to account for the enhanced memory-dip is based on the observation that the interaction-to-disorder ratio plays a role in the magnitude of the memory-dip and on the realization that this ratio

increases in the PPC-state relative to the dark-state.

That the visibility of the memory-dip is a function of the ratio of Coulomb-interaction I_C to disorder W should be clear; recall that this modulation in $G(V_g)$ has its roots in the competition between interaction and disorder: The memory-dip vanishes when disorder is small, and it is obviously absent altogether when interaction is turned-off. It is then intuitively expected that the memory-dip is most conspicuous when the disorder and interaction are comparable in magnitude.

The first point we wish to make here is that, over the range of parameters relevant for *all* the electron-glasses studied to date, $I_C \gg W$.

The magnitude of the interparticle Coulomb interaction I_C for a system with a given N can be expressed by:

$$I_C = \frac{e^2}{\epsilon r} = \frac{e^2 N^{1/3}}{\epsilon} \quad (2)$$

where ϵ is the dielectric constant of the medium and $r = N^{-1/3}$ is the interparticle average spacing. The disorder required to make the system strongly-localized (the pre-condition for being in the electron-glass phase [27]) :

$$W \approx 6.5 \cdot E_F \quad (3)$$

and using free-electron formula this may be cast in terms of carrier-concentration:

$$W \approx 6.5 \cdot \frac{\hbar^2 k_F^2}{2m^*}; \text{ and } k_F = (3\pi^2 N)^{1/3} \quad (4)$$

Note that all currently known electron-glasses have carrier-concentration in the range $2 \times 10^{19} \text{cm}^{-3} \leq N \leq 5 \times 10^{21} \text{cm}^{-3}$. As explained in [27], systems with higher carrier-concentration than $N \approx 10^{22} \text{cm}^{-3}$ are difficult to strongly-localize unless by making granular, and the disorder in systems with $N \leq 10^{19} \text{cm}^{-3}$ is too weak to reduce transition rates sufficiently as to afford observation of the memory-dip (this is the reason for the failure of lightly-doped semiconductors to exhibit a memory-dip [27]).

The values for W and I_C may now be estimated using Eq.2 and Eq.4 with the parameters for indium-oxide which has been studied over the widest range of carrier-concentration among all electron-glasses. Taking the dielectric constant as $\epsilon=10$, and effective mass $m^*=0.3m_0$ one gets: $I_C/W \approx 0.14$ and $I_C/W \approx 0.025$ for In_xO samples with $N \approx 4 \times 10^{19} \text{cm}^{-3}$ and $N \approx 5 \times 10^{21} \text{cm}^{-3}$ respectively. These represent the two extreme limits in N over which electron-glasses were studied. The memory-dips associated with these limit- N values are plotted in Fig.18 illustrating the much larger $\delta G_{\text{MD}}/G_0$ exhibited by the sample with the larger I_C/W ratio.

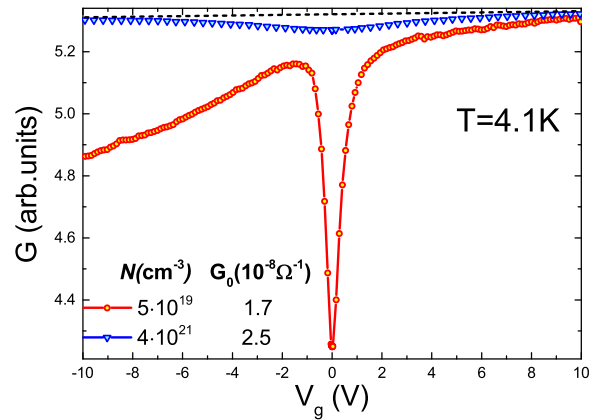


FIG. 18: Field-effect sweeps comparing the memory-dip of two In_xO samples with different values of N (obtained by different In/O composition) but similar R_{\square} and measured under identical conditions (sweep rate, relaxation history). These $G(V_g)$ plots are based on the same field-effect structures described in section II but with $0.5 \mu\text{m}$ SiO_2 spacer. Dashed line is the assumed thermal-DOS plotted to expose the wide and shallow memory-dip of the sample with the larger N . The latter has $\delta G_{\text{MD}}/G_0 \approx 1.1\%$ while the low N sample exhibits $\delta G_{\text{MD}}/G_0 \approx 21\%$.

With these parameters for In_xO , the interaction-to-disorder ratio $I_C/W \approx 1$ would be obtained for an Anderson insulator with carrier-concentration $N \approx 3 \times 10^{16} \text{cm}^{-3}$. This N is well below the concentration where the relaxation time becomes too short for observation of electron-glass features by standard field-effect techniques. Note that it is the system with the lower N that has the larger I_C/W (and consequently larger $\delta G_{\text{MD}}/G_0$). This is so because $I_C \propto N^{1/3}$ while for electron-glasses $W \propto N^{2/3}$, thus I_C/W actually decreases with N . In other words, all other things being equal, higher carrier-density means stronger Coulomb interaction but even stronger disorder.

Large values for $\delta G_{\text{MD}}/G_0$, of the order of 15-30% (for $R_{\square} \approx 10 \text{M}\Omega$ at 4K), are routinely obtained using the crystalline version of indium-oxide ($\text{In}_2\text{O}_{3-x}$) that also has low carrier-concentration $N \approx 4 \times 10^{19} \text{cm}^{-3}$ [12]. On the other hand, electron-glasses with $N \geq 10^{21} \text{cm}^{-3}$ typically show $\delta G_{\text{MD}}/G_0$ of the order of $\approx 1\%$ in samples with comparable R_{\square} . This is manifestly the case for the GeBi_xTe_y films studied here (see Fig.6 above).

The larger δG_{MD} observed in the PPC-state in both GeBi_xTe_y and the GeSb_xTe_y alloys may just be another example of the dependence of the memory-dip magnitude on I_C/W . Note that the enhanced conductivity in the PPC-state is mainly due to higher concentration of carriers N created by the optical excitation. Being in the strongly-localized regime, the system lacks metallic screening and therefore higher N means an increase in the interparticle-interaction I_C . It is less clear what, if any, is the accompanying change of disorder; The defect that hinders recombination in the PPC-state is presumed to

be stabilized by a spatial-shift Δx of an atom, and possibly a change in the local charge [8]. The atomic displacement Δx , is sub-atomic [8] and thus much smaller than the localization-length which can hardly affect the perceived ionic-disorder. The scattering cross-section may however be different due to a change in the local charge in the PPC-state, but this may go either way. It is then plausible to assume that, in the PPC-state, the ratio of Coulomb-interaction to disorder is larger than in the dark-state. In that case the enhanced $\delta G_{MD}/G_0$ in the PPC-state just follows a trend generally obeyed by all electron-glasses with $N \geq 3 \times 10^{19} \text{cm}^{-3}$.

To summarize, we presented in this paper experimental results that demonstrate coexistence of persistent-photoconductivity and electron-glass features in the degenerate semiconductor GeBi_xTe_y . Both phenomena exhibit sluggish conductance relaxation albeit due to different mechanisms. The conductance in the persistent-state is associated with the recombination of optically-generated excess charge. The process is slow presumably due to an energy-gap induced by a local structure re-arrangement. The different PPC susceptibility of the system to the nature of the element added to the alloy may help in identifying the microscopic mechanism involved.

The electron-glass dynamics, on the other hand, is associated with a change in the carriers *mobility* rather than carrier-concentration, and it is controlled by the combined effects of quench-disorder and variety of interaction-related mechanisms: Many-body effects, and several variations of the orthogonality-catastrophe [40–42] may further extend relaxation times. These phenomena demonstrate the richness and complexity of electronic transport in disordered and interacting quantum systems. The current study re-affirms the notion that electron-glasses with long relaxation times are inherent property of Anderson insulators where disorder is much larger than the Coulomb interaction.

The enhancement of the memory-dip magnitude induced by infrared radiation lead us to the conjecture that this feature of the electron-glass is controlled by the ratio of interaction and disorder. This was shown to be consistent with a number of experiments. Further experimental work needs to be done to test this trend in different materials. The magnitude $\delta G_{MD}/G_0$ of the memory-dip is a more complicated issue to characterize than the width Γ . At a given temperature, Γ depends only on carrier-concentration of the system [12]. The magnitude of the memory-dip, on the other hand, depends on many other factors; $\delta G_{MD}/G_0$ depends on the rate of sweeping the gate-voltage V_g , it depends on the time the sample equilibrated under V_g (history), and it depends on the R_{\square} and on the sample thickness. In addition it may vary between different preparation batches (which suggest influence of structural details). The functional dependence of $\delta G_{MD}/G_0$ on carrier-concentration is therefore not yet es-

tablished. Nevertheless, the overall trend that $\delta G_{MD}/G_0$ increases when the carrier-concentration decreases (in the regime $I_C \ll W$) is clear enough. Some insight on this issue may come from numerical simulations looking at how the I_C/W ratio affects the memory-dip magnitude using the method of Meroz et al [25]; in principle using this technique should allow probing the regime where the interaction is larger than the disorder, which is hard to implement experimentally.

Illuminating discussions with Ady Vakin on the electron-glass dynamics and with Dmitry Khokhlov on persistent-photoconductivity are gratefully acknowledged. This research has been supported by a grant No 1030/16 administered by the Israel Academy for Sciences and Humanities.

-
- [1] Marcos Rigoll, Vanja Dunjko, and Maxim Olshanii, *Nature*, **452**, 854 (2008).
 - [2] Anatoli Polkovnikov, Krishnendu Sengupta, Alessandro Silva, and Mukund Vengalattore, *Rev. Mod. Phys.* **83**, 863 (2011).
 - [3] N. G. Ptitsina, G. M. Chulkova, K. S. Il'in, A. V. Sergeev, F. S. Pochinkov, E. M. Gershenson, and M. E. Gershenson, *Phys. Rev. B* **56**, 10089 (1997).
 - [4] B. A. Akimova, V. Dmitriev, R. Khokhlov, L. I. Ryabova, *phys. stat. sol. (a)* **137**, 9 (1993).
 - [5] T. Y. Lin, H. M. Chen, M. S. Tsai, and Y. F. Chen, F. F. Fang, C. F. Lin and G. C. Chi, *Phys. Rev. B* **58**, 13793 (1998).
 - [6] H. J. Queisser and D. E. Theodorou, *Phys. Rev. Lett.*, **43**, 401 (1979); Jennifer Misuraca, Jelena Trbovic, Jun Lu, Jianhua Zhao, Yuzo Ohno, Hideo Ohno, Peng Xiong, and Stephan von Molnár, *Phys. Rev. B* **82**, 125202, (2010).
 - [7] P. M. Mooney, *Journal of Applied Physics* **67**, R1 (1990); Z. Su and J. W. Farmer, *Appl. Phys. Lett.* **59**, 30 (1991); D. Jia, J. Zhu, and B. Wu, *Journal of The Electrochemical Society*, **147** (1) 386 (2000).
 - [8] D. V. Lang and R. A. Logan, *Phys. Rev. Lett.*, **39**, 635 (1977); D. V. Lang, R. A. Logan, and M. Jaros, *Phys. Rev. B* **19**, 1015 (1979). The notion of a gap created by an atom-shift, which is central to the model, was first used by R. W. Gurney and N. F. Mott, in *Trans. Faraday Soc.* **35**, 69 (1939).
 - [9] Z. Ovadyahu, *Phys. Rev. B.* **91**, 094204 (2015).
 - [10] By "intrinsic" we mean that the glassy effects appear in a given substance *independently* of the way the sample was prepared to achieve the required parameters (resistivity at the measuring temperature, carrier-concentration, and dimensionality). Most importantly, the system has to exhibit a memory-dip with a width that is commensurate with the carrier-concentration of the material.
 - [11] Z. Ovadyahu, *Phys. Rev. Lett.*, **115**, 046601 (2015).
 - [12] Z. Ovadyahu, *Phys. Rev. B* **78**, 195120 (2008).
 - [13] U. Givan and Z. Ovadyahu, *Phys. Rev. B* **86**, 165101 (2012).
 - [14] Z. Ovadyahu, *Phys. Rev. B.* **94**, 155151 (2016).
 - [15] A. Vakin, Z. Ovadyahu, and M. Pollak, *Phys. Rev. B*

- 65**, 134208 (2002).
- [16] A. H. Edwards A. C. Pineda, P. A. Schultz, M.s G. Martin, A. P. Thompson, and H.P. Hjalmarsen, C. J. Umrigar, J. Phys.: C Condens. Matter **17**, L329 (2005); *ibid* Phys. Rev. B **73**, 045210 (2006).
- [17] J. H. Davies, P. A. Lee, and T. M. Rice, Phys. Rev. Letters, **49**, 758 (1982).
- [18] M. Grünewald, B. Pohlman, L. Schweitzer, and D. Würtz, J. Phys. C, **15**, L1153 (1982).
- [19] M. Pollak and M. Ortuño, Sol. Energy Mater., **8**, 81 (1982); M. Pollak, Phil. Mag. B **50**, 265 (1984).
- [20] G. Vignale, Phys. Rev. B **36**, 8192 (1987).
- [21] Ariel Amir, Yuval Oreg, and Yoseph Imry, Annu. Rev. Condens. Matter Phys. **2**, 235 (2011); M. Pollak, M. Ortuño and A. Frydman, "The *Electron Glass*", Cambridge University Press, England (2013).
- [22] C. C. Yu, Phys. Rev. Lett., **82**, 4074 (1999).
- [23] Eran Lebanon, and Markus Müller, Phys. Rev. B **72**, 174202 (2005).
- [24] R. Gempel, Europhys. Lett., **66**, 854 (2004).
- [25] Y. Meroz, Y. Oreg and Y. Imry, EPL, **105**, 37010 (2014).
- [26] P. A. Lee, Phys. Rev. B **26**, 5882 (1982).
- [27] Z. Ovadyahu, Phys. Rev. B. **95**, 134203 (2017).
- [28] A. Vaknin, Z. Ovadyahu, and M. Pollak, Phys. Rev. Lett., **81**, 669 (1998).
- [29] Z. Ovadyahu, X. M. Xiong, and P. W. Adams, Phys. Rev. B **82**, 195404 (2010).
- [30] A. Vaknin, A. Frydman, Z. Ovadyahu, and M. Pollak, Phys. Rev. B **54**, 13604 (1996).
- [31] N. Apsley and H.P. Hughes, Philos. Mag. **31**, 1327 (1975).
- [32] M. Pollak and I. Riess, J. Phys. **C9**, 2339 (1976).
- [33] R. M. Hill, Philos. Mag. **24**, 1307 (1971).
- [34] B. I. Shklovskii, Fiz. Tekh. Poluprovodn. **6**, 2335 (1972) [Sov.Phys. Semicond. **6**, 1964 (1973)].
- [35] Z. Ovadyahu, Phys. Rev. Lett., **108**, 156602 (2012).
- [36] I. Schwartz, S. Shaft, A. Moalem and Z. Ovadyahu, Phil. Mag. B **50**, 221 (1984).
- [37] Z. Ovadyahu, Phys. Rev. Lett., **108**, 156602 (2012).
- [38] V. Orlyanchik, and Z. Ovadyahu, Phys. Rev. Lett., **92**, 066801 (2004).
- [39] V. Orlyanchik, A.Vaknin, Z. Ovadyahu, and M. Pollak, Phys. Stat. Sol., B **230**, 61 (2002).
- [40] Z. Ovadyahu, Phys. Rev. Lett., **99**, 226603 (2007).
- [41] Vedika Khemani, Rahul Nandkishore, and S. L. Sondhi, Nature Physics, **11**, 560 (2015).
- [42] D. L. Deng, J. H. Pixley, X Li, S. D. Sarma, Phys. Rev. B. **92**, 220201(R) (2015).